Int J Comput Vis manuscript No.
(will be inserted by the editor)

RSLAM: A System for Large-Scale Mapping in Constant-Time using Stereo

Christopher Mei · Gabe Sibley · Mark Cummins · Paul Newman · Ian Reid

Received: date / Accepted: date

Abstract Large scale exploration of the environment requires a constant time estimation engine. Bundle adjustment or pose relaxation do not fulfil these requirements as the number of parameters to solve grows with the size of the environment. We describe a relative simultaneous localisation and mapping system (RSLAM) for the constant-time estimation of structure and motion using a binocular stereo camera system as the sole sensor. Achieving robustness in the presence of difficult and changing lighting conditions and rapid motion requires careful engineering of the visual processing, and we describe a number of innovations which we show lead to high accuracy and robustness. In order to achieve real-time performance without placing severe limits on the size of the map that can be built, we use a topometric representation in terms of a sequence of relative locations. When combined with fast and reliable loop-closing, we mitigate the drift to obtain highly accurate global position estimates *without* any global minimisation. We discuss some of the issues that arise from using a relative representation, and evaluate our system on long sequences processed at a constant 30-45 Hz, obtaining precisions down to a few meters over distances of a few kilometres.

Keywords SLAM · Stereo · Tracking · Loop Closing · SIFT

1 Introduction

Building autonomous platforms using vision sensors has encouraged many developments in low-level image processing and in estimation techniques. Recent improvements have lead to real-time solutions on standard hardware. However these often rely on global solutions that do not scale with the size of environment. Furthermore, few systems integrate loop closure or a relocalisation mechanism that is essential for working in non-controlled environments where tracking assumptions are often violated. In this work, we investigate how to efficiently combine relevant approaches to obtain a vision-based solution that provides high frame rate, constant-time exploration, resilience to motion blur and a relocation and loop closure mechanism.

Vision-based systems can be classified between monocular and stereo solutions. The presence of a single camera on an increasing amount of consumer goods (mobile phones, personal digital assistants, laptops, etc.) is a strong motivation for research in monocular vision. However the use of a monocular system can lead to failure modes due to non-observability (e.g. with pure rotation), problems with scale propagation and requires extra computation to provide depth estimates. To avoid these issues, the current system uses a stereo pair which paradoxically reduces the computation as low-level processing can take advantage of scale (Section 6) and rely less on expensive joint depth and pose estimation.

The relative SLAM system presented in this paper combines a world representation enabling loop closure in real-time (Section 3) with carefully engineered low-level image processing adapted to stereo image pairs. The novelty in the world representation comes from the continuous relative formulation that avoids map merging and the transfer of statistics between sub-maps. We describe a scheme for relative bundle adjustment (RBA) within this framework that leads to improved precision in Section G. In this article, we demonstrate the integration of three key components: (i) a represen-

C. Mei, G. Sibley, M. Cummins, P. Newman and I. Reid
Robotics Research Group, Department of Engineering Science, Parks Road, Oxford, OX1 3PJ
E-mail: {cmei,gsibley,mjc,pnewman,ian}@robots.ox.ac.uk

tation of the global environment in terms of a *continuous* sequence of relative locations; (ii) a visual processing front-end that tracks features with sub-pixel accuracy, computes temporal and spatial correspondences, and estimates precise local structure from these features; (iii) a method for loop-closure which is independent of the map geometry, and solves the loop closure and kidnapped robot problem; to produce a *system* capable of mapping long sequences over large distances with high precision, but in constant time.

The remainder of the article is structured as follows. After a section on related work, we discuss the representation of the environment chosen in this work and how it relates to standard methods in computer vision and robotics. In Section 6 we investigate the notion of "true scale" or how a stereo pair can provide an efficient approach to generating scale-invariant descriptors. Section 4 then describes the different visual processing steps to estimate the position of the camera and build the map from the stereo images. Section 5 addresses the problems of relocalisation (i.e. how to recover when tracking fails) and loop closure (i.e. how to recognise a previously mapped region). Finally, we analyse the performance of the system on simulated and large-scale indoor and outdoor sequences.

2 Related work

In this section, we will discuss specifically recent advances in visual SLAM (Simultaneous Localisation and Mapping) with a focus on stereo systems. A broader survey of SLAM approaches can be found for example in (Thrun et al (2005); Durrant-Whyte and Bailey (2006); Bailey and Durrant-Whyte (2006)).

Visual SLAM has seen many successful systems in recent years. Several approaches have been proposed for estimating the motion of a single camera and the structure of the scene in real-time. The application of an Extended Kalman Filter (EKF) to this problem yielded one of the earlier real-time monocular SLAM systems (Davison (2003); Davison et al (2007)). However the EKF suffers from a number of problems which have proven limiting:

- the number of landmarks that can be processed is limited to a few hundred due to quadratic complexity of the EKF. Bundle adjustment (Triggs et al (1999)) has a complexity linear in the number of landmarks (but cubic in the number of poses) enabling the processing of more landmarks.
- consistency. EKF is known to produce inconsistent estimates (Julier and Uhlmann (2001)), one of the weaknesses being the impossibility of relinearising the cost function after marginalisation.

These reasons have lead recent real-time monocular systems to use local (Mouragnon et al (2006)) or global (Klein and Murray (2007); Eade and Drummond (2007, 2008)) bundle adjustment as the underlying estimator. A careful choice of key-frames is however required to keep the solving tractable. Compared to our present work, (Mouragnon et al (2006)) does not provide a loop closing mechanism and cannot as such reduce drift when returning to a previously explored region. (Klein and Murray (2007)) is a system aimed at small environments with applications in augmented reality. It uses a separate thread for bundle adjustment enabling the building of accurate maps but is not adapted to large scale exploration. (Eade and Drummond (2007, 2008)) share strong similarities with the present work combining a relative representation and a non-probabilistic loop closure mechanism. In this work however, the low-level image processing is adapted to stereo vision and the focus is on precise exploration without global graph minimisation.

Recent research has also provided some real-time solutions using stereo pairs (Nistér et al (2006); Konolige and Agrawal (2008)). In (Nistér et al (2006)), the authors rely on local bundle adjustment using a global representation but do not address the problem of loop closing. The closest related work is the FrameSLAM system by Konolige and Agrawal (Konolige and Agrawal (2008)). FrameSLAM and the current system differ mainly in the objective: FrameSLAM focuses on reducing the complexity of large-scale solving whereas we aim at providing a *locally* accurate map and trajectory using relative bundle adjustment with a bounded complexity (Section G). As such, the complexity of FrameSLAM grows with the size of the environment (albeit slowly) whereas the current approach is constant-time. For many applications (path planning, object manipulation, dynamic object detection, ...) good local accuracy is sufficient and we show that it can be recovered in constant time (the complexity being related to the size of the working space). It is also important to note that global metric maps and relative maps are not equivalent (see Section 3.2) and share different properties.

3 Map representation

In this section, we introduce our Continuous Relative Representation (CRR), used to represent the location of map features with respect to the current sensor position. Since it differs in subtle but important ways from

the prior art, we begin with a review of representations that have been used previously with some success.

3.1 World representations

The position of the robot and the landmarks representing the environment can be represented in different ways (Fig. 1):

Global coordinates. (Fig. 1(a)) The most common representation is to a fix an arbitrary initial frame (usually set to be the identity transform) and represent all subsequent position and landmark estimates with respect to this frame.

Robo-centric coordinates. (Fig. 1(b)) This is similar to using global coordinates but the initial frame is chosen to be the current robot position. The map has to be updated at each new position estimate. This representation has been shown to improve consistency for EKF SLAM estimation (Castellanos et al (2004)).

Relative representation. (Bosse et al (2004); Eade and Drummond (2008); Konolige and Agrawal (2008); Moore et al (2009)). (Fig. 1(d),1(e)) In this framework, each camera position is connected by an edge transform to another position forming a graph structure. There is no privileged position and recovering landmark estimates requires a graph traversal (e.g. breadth first search or shortest path computation).

Sub-maps. (Fig. 1(c), 1(d)) Sub-maps consist in representing a map by local frames and can be used with any of the previously discussed map representations. There are mainly two reasons for using sub-maps: reducing the computation and improving the consistency (mainly in filtering frameworks to reduce the effect of propagating inconsistent statistics).

In the presented system, the robot position and map are represented in a *continuous* relative framework (CRR) (Fig. 1(e)).

Several related methods have been described in the literature. In the recent work by Moore *et al* (Moore et al (2009)), the authors provide a representation similar to a CRR without graph exploration. The authors do not address the problem of refining local estimates and do not discuss loop closure. The representation is used to fuse global low-frequency measurements (e.g. GPS at 1Hz) with high frequency local estimates (provided for example by an inertial measurement unit at 100Hz). Compared to the present approach, this work is aimed at providing stable motion estimates for robot navigation and the focus is less on the mapping aspect of the problem. In the works by Bosse *et al* (Bosse et al (2004)) and Eade and Drummond (Eade and Drummond (2008)) information is fused locally into sub-maps that are connected by relative transforms as in Fig. 1(d). Fusing information leads to a number of difficulties: (i) map-merging is required at loop closure (Bosse et al (2004)) (ii) computing a global solution can become expensive due to the locally dense covariance structures produced by marginalisation and (iii) it is no longer possible to benefit from better precision and consistency by relinearisation. Furthermore, as explained in the following section, choosing what information to merge can be hard and have a strong impact on the final results. In contrast, relative bundle adjustment (Section G) using a CRR framework has the advantages of standard bundle adjustment (a sparse Hessian structure and the possibility of relinearising) and does not require a complex map-merging step at loop closure. This representation can be seen as the limit of a sub-mapping approach when the size of the local map is reduced to containing a single frame.

3.2 Continuous Relative Representation (CRR)

Terminology The following terms are used to describe different aspects of the CRR:

- a **base frame** is defined as the pose in which a landmark is represented (i.e. where its 3-D coordinates are kept),
- an **active region** corresponds to the set of poses within a given distance in the graph to the current pose.

A continuous relative representation (CRR) was chosen to represent the world as described in Fig. 2. During the exploration of the environment, each new pose of the robot becomes a vertex in a graph connected by an edge representing the estimated transform between poses. In Fig. 2, this edge is indicated by a continuous line. The active region contains the set of poses within a given distance in the graph to the current pose. In the example, an active region of size two was chosen. Generally, the active region will be comprised of the latest poses. However, in the case of a loop closure, as illustrated by Fig. 2(b), older poses will also form the active region.

The active region defines the landmarks visible from the current frame. Representing the local environment around the robot consists in projecting the active region into the current frame. Landmarks with base frames (where the landmark's 3-D coordinates are kept) belonging to poses from the active region are projected into the current frame by composing the transforms

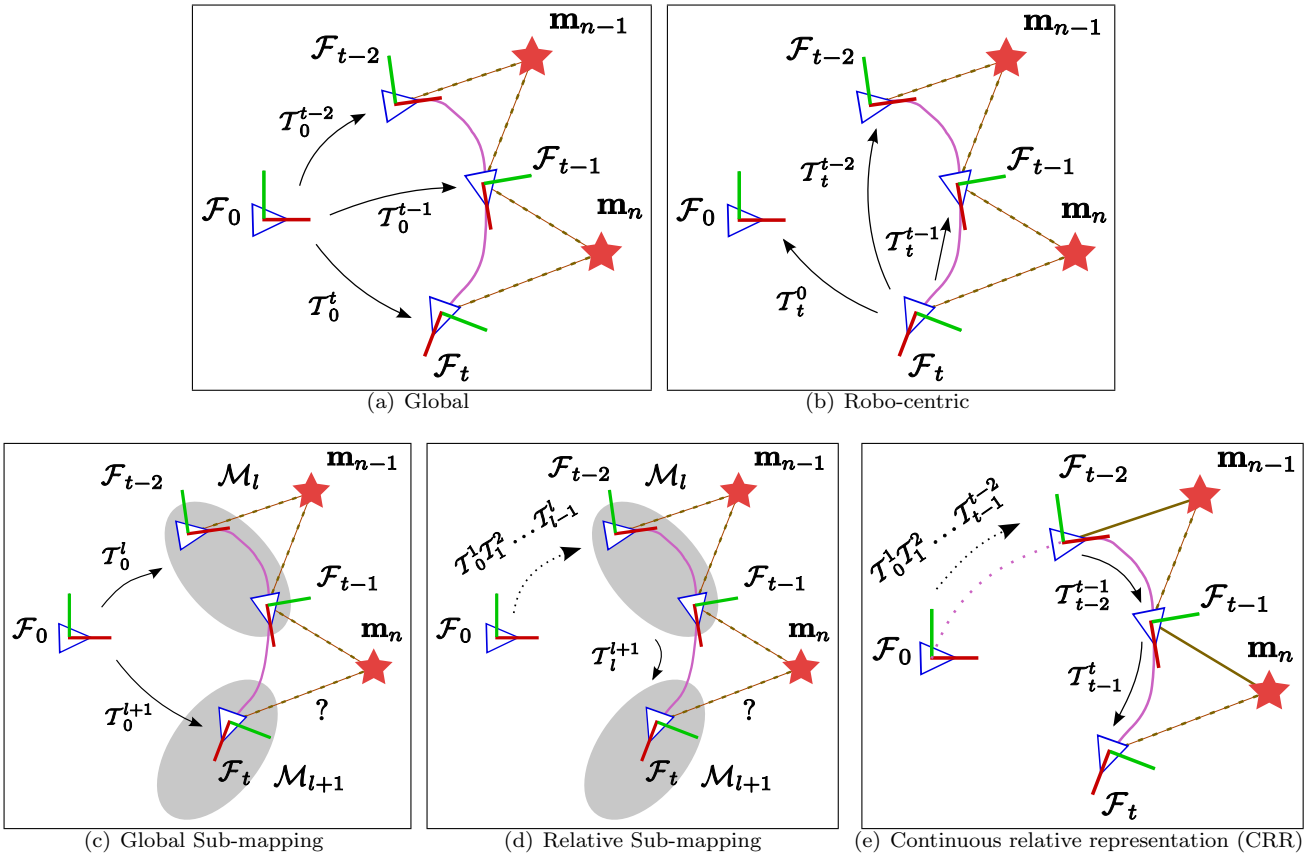

Fig. 1 Different pose and landmark representations with $\mathbf{m}$ for landmarks, $\mathcal{F}$ for frames, $\mathcal{T}$ for transforms and $\mathcal{M}$ for sub-maps where applicable. Dashed lines represent measurements. Landmarks are connected to their base frames by filled lines. '?' indicates the difficulty in sharing information between sub-maps. In relative sub-mapping (d), sub-maps (represented by a shaded area) represent the landmark position locally with respect to a privileged frame. In the proposed continuous relative representation (e), there is no sub-map and any frame can be a base-frame.

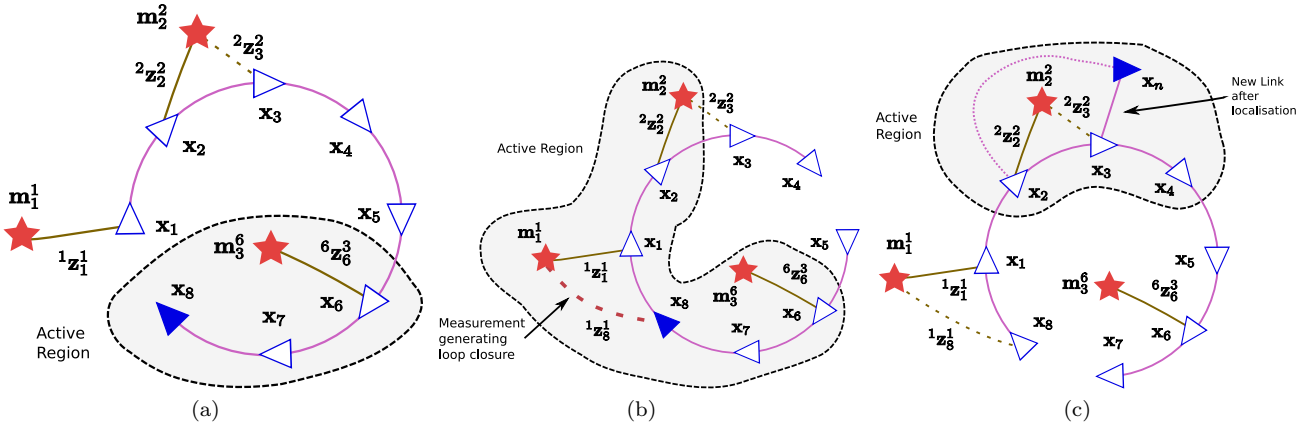

Fig. 2 Relative representation. Triangles represent robot poses ($\mathbf{x}_i$) with the current pose filled in. Stars represent landmarks, $\mathbf{m}_i^j$ is the ith landmark in the system represented in base-frame j. ${}^k\mathbf{z}_i^j$ indicates a measurement of landmark j from frame i with base frame k. (a) Graph representing a robot trajectory. The active region of size two contains the latest two poses. (b) Trajectory after loop closure. The robot in $\mathbf{x}_9$ makes an observation of landmark $\mathbf{m}_1$. This provides an estimate between poses $\mathbf{x}_1$ and $\mathbf{x}_9$ represented by the new link in the graph. The active region of size two, discovered by breadth first search in the graph, now comprises the older poses $\mathbf{x}_1$ and $\mathbf{x}_2$ because of the added link. The link between $\mathbf{x}_4$ and $\mathbf{x}_5$ still exists but is no longer represented as we do not enforce the composition of the transforms along cycles to be the identity. (c) Trajectory after localisation. The robot was previously connected to $\mathbf{x}_2$ but the latest estimate of its position to the poses in the active region has shown a closer proximity to $\mathbf{x}_3$. In this case, the old link is discarded and a new link is created, here between $\mathbf{x}_n$ and $\mathbf{x}_3$.

along the edges. For example, in Fig. 2(a), projecting landmark $\mathbf{m}_3$ (the upper script is used here to indicate that it is represented in frame 6) in the current frame will require to compose through $\mathbf{x}_7$: $\mathbf{m}_3^8 = \mathcal{T}_8^7 \mathcal{T}_7^6 \mathbf{m}_3^6$. In this work, the discovery of the active region is made by a breadth first search (BFS). A probabilistic approach could also be used with a Dijkstra shortest path discovery using the covariance from the edge transformations, but previous research has shown a negligible improvement over the map quality (Bosse et al (2004)).

The projected estimates (or local map) can be used for obstacle avoidance, grasping or in this work to establish matches and compute the position of the robot. In the current setting we do not use the uncertainty provided by the estimates for the data association but use a fixed-size window. In this framework, loop closure consists in creating a new edge that can then be used to transfer 3-D landmark estimates into the current frame and therefore evaluate their projection in the image (Fig. 2(b)).

It should be noted that the global solution minimising the reprojection error in a relative framework is not equivalent to the global solution using a global reference with the same measurements. In the case of unobservable ego-motion (e.g. if the robot uses a means of transport such as a lift or car), the map cannot be represented in a Euclidean setting. Methods that use a global frame would fail but a relative representation still holds. This would also be the case when sub-mapping with a local map that overlaps such regions. This observation leads to a change in perspective where the importance of detecting changes in the environment becomes apparent as imposing global constraints blindly (such as those imposed in a pose relaxation framework) would degrade the accuracy of the map.

3.3 Relative Bundle Adjustment (RBA)

Bundle adjustment computes the optimal (maximal likelihood function under the assumption of Gaussian uncertainty) structure and motion from a set of corresponding image projections. It is a well studied problem in the context of a single global coordinate frame (Triggs et al (1999)).

The cost function minimises the reprojection between landmark $\mathbf{m}_i$ and its measurements $\mathbf{z}_i^j$ in image j for all M_i images and all N landmarks. Let $Proj_j$ be the projection of $\mathbf{m}_i$ in image j. In a global frame, $Proj_j$ is a function of the position of frame j with respect to the origin. Assuming the measurement $\mathbf{z}^j$ is normally distributed $\mathbf{z}_i^j \sim \mathcal{N}(Proj_j(\mathbf{m}_i), \Sigma_{i,j})$, we obtain:

$$F = \sum_{i=1}^{N} \sum_{j=1}^{M_i} (\mathbf{z}^i - Proj_j(\mathbf{m}_i))^\top \Sigma_{i,j}^{-1} (\mathbf{z}^i - Proj_j(\mathbf{m}_i))$$

The computation of the reprojection error in a CRR framework differs from the computation in a global coordinate frame as each landmark estimate requires the traversal of the graph along the kinematic chains linking the base-frame to the images observing the landmark. (This traversal corresponds to the computation of a metric on the manifold defined by the trajectory frames in the graph.)

In other words, in this context, the projection function $Proj_j$ now also depends on the base-frame k of landmark $\mathbf{m}_j^k$ and thus on all the transforms linking the two frames:

$$Proj_{j,k} = f(\mathcal{T}_k^j) = f(\mathcal{T}_k^{k-1}, \mathcal{T}_{k-1}^{k-2}, \ldots, \mathcal{T}_{j+2}^{j+1}, \mathcal{T}_{j+1}^{j})$$

As with standard bundle adjustment, this problem is solved using Gauss-Newton minimisation. As discussed in the previous section, this cost function has a different minimum to the standard approach. Furthermore the sparsity pattern is changed. However sparsity remains which is key to solving the problem in real-time. In (Sibley et al (2009)), we consider in much greater detail the implications of the CRR and RBA. In particular, we present empirical evidence that strongly suggests this remains a constant-time algorithm.

4 Stereo visual processing

This section describes the different steps applied to processing stereo image pairs. It is similar to other works in the literature (Nistér et al (2006); Klein and Murray (2007)), the main novelty is in: a) the systematic application of second-order minimisation (Benhimane and Malis (2004); Mei et al (2008)) for the pose initialisation and sub-pixel refinement, b) the use of quadtrees to ensure adequate spreading of the features in the image and c) the use of true scale (Section 6) to build discriminative descriptors at a lower cost than the standard scale-space computation combined with a descriptor (as in SIFT (Lowe (2004))).

We begin with a top level view. For each incoming frame, the following steps are made:

A image pre-processing,
B feature extraction,
C pose initialisation through sum-of-squared difference (SSD) inter-frame tracking,
D temporal feature matching: the features are matched with current 3-D landmark estimates (the map),

E localisation: the position of the camera pair is estimated by minimising the landmark to image reprojection error,
F left-right matching: new 3-D landmarks are initialised by matching image templates between the left and right images along scanlines and triangulating the results.
G relative bundle adjustment.

We will discuss in detail the different processing steps.

A Image pre-processing

Each incoming image is rectified using the known camera calibration parameters to ensure efficient scanline searches of corresponding left-right matches (Hartley and Zisserman (2000)). The image intensities for left and right images are then corrected to obtain the same mean and variance. This step improves the left-right matching scores, enabling better detection of outliers. A scale-space pyramid of both images is then built using a box filter with one image per octave for computational efficiency. Using a pyramid yields features at different scales, giving greater resilience to focus and motion blur. It is also used for the pose initialisation and the calculation of SIFT descriptors.

B Feature extraction

The feature locations used in this work are provided by the FAST corner extractor (Rosten and Drummond (2005)) that provides good repeatability at a small computational cost. To obtain resilience to blur and enable matching over larger regions in the image, FAST corners are extracted at different levels of the scale-space computed in the previous step. In practise, we used three pyramid levels in processing indoor sequences, but found that two levels were sufficient for our outdoor sequences; the type of camera, and the amount of motion blur expected are factors which influence this parameter.

The corner extraction threshold is initially set at a value providing a compromise between number of points and robustness to noise. This threshold is then decreased or increased at each time-step to ensure a minimal number of points. This proved sufficient to adapt to the strong changes in illumination and low contrast typically encountered in outdoor sequences.

C Pose initialisation with image-based gradient descent

The apparent image motion of features in visual SLAM is typically dominated by the ego-rotation, and large inter-frame rotation is a common failure mode for systems based on an inter-frame feature search. To improve robustness, an estimate of the 3-D rotation is obtained using the algorithm described in (Mei et al (2008)) at the highest level of the scale-space pyramid for efficiency and to widen the basin of convergence. This algorithm minimises the sum-of-squared-distance of image intensity using a second-order gradient descent minimisation (ESM). The obtained estimate is then used to guide the search for temporal feature correspondences.

The complexity of the tracking algorithm is $O(p^2 n)$ with p the number of parameters ($p = 3$ for a rotation) and n the number of pixels. The following timings for one iteration were obtained for the architecture described in Section 7.5:

32×24	64×48	128×96
0.16ms	0.58ms	2.16ms

On average, 4 iterations were required to converge. In the tested sequences an image of size 32×24 was used for tracking.

D Temporal feature matching

The current 6-DOF pose is initialised to the rotation computed in the previous stage, and a translation of zero relative to the previous pose. The 3-D coordinates of the landmarks (i.e. the map) computed through the graph representing the relative poses (as detailed in Section 3.2) are then projected into the left and right images of the current stereo pair and matched in a fixed-sized window to the extracted FAST corners using mean SAD (sum of absolute difference with the mean removed for better resilience to lighting changes) on image patches of size 9×9. This step is then followed by image sub-pixel refinement using ESM. Matches whose score fall below a threshold after ESM are rejected. Applying this threshold after sub-pixel refinement provides a more meaningful comparison as patches with high frequency will typically have high errors before the sub-pixel refinement. The influence of sub-pixel refinement over the accuracy of the motion estimates will be evaluated in Section 7.

E Localisation

After the map points have been matched, 3-point pose RANSAC (Fischler and Bolles (1981); Nistér et al (2006))

is applied to obtain an initial pose estimate and outlier classification. The total reprojection error over both views is then minimised using m-estimators for robustness (this minimisation can be found in standard textbooks (Hartley and Zisserman (2000))). After the minimisation, landmark measurements with strong reprojection errors are removed from the system. This step proved important to enable early removal of outliers and the possibility of adding new, more stable, landmarks.

F Initialising new features

To achieve good accuracy at a high frame-rate we aim to measure between 100-150 features, with a fairly even spatial distribution across the image, at every time-step. Thus after temporal matches have been established we seek to initialise new features in the current frame. The feature selection process uses quadtrees, described in following subsection, to ensure a uniform distribution of the features. Information theory could also be used to select features that constrain the motion estimation and for setting the search region for tracking (Chli and Davison (2008)) but the quadtree approach proved sufficient in the tested sequences.

Along with each feature track, an image patch (of size 9×9) is saved for sub-pixel matching in time and a SIFT descriptor is computed for robust relocalisation and loop closure (Section 5).

Feature selection using quadtrees

The feature selection process follows the assumption that we desire distinctive features with a uniform distribution in the image (irrespective of the underlying tracking uncertainty). A quadtree is used to represent the distribution of the measurements at each time step. It contains the number of measurements in the different parts of the image and the maximal amount of points allowed, to ensure a uniform distribution of features. It is used in the following way:

1. In Step D., the matched map points increment the quadtree count according to their measurement image locations.
2. To add new features, FAST corners are extracted from the left and right images and ordered by a distinctiveness score (in this work we used Harris scores). To decide which features to add, the best features are taken in order and their image location is checked in the quadtree to ensure the maximal amount of allowed points has not been exceeded. If it passes the test, a match is sought along the corresponding epipolar line (scan-line). This search begins by looking for a suitable FAST corner on this line. However if this fails, we perform a dense SAD search, seeking the patch along the scan-line that correlates best with the feature patch. Although slower, this enables us to initialise features where FAST has fired only in one of the images. This allows us to put features in areas that provide good constraints for motion estimation although the corner response is weak. The precision of final match is then improved by sub-pixel second-order minimisation (Benhimane and Malis (2004)) over the image coordinates and the average intensity (three parameter minimisation).

G Relative bundle adjustment

The final step to improve the local estimates is to apply relative bundle adjustment. Near optimal parameter estimates lead to longer feature tracks, resilience to higher reprojection errors, less clutter and lower memory usage. This final refinement step is important and experimentally was shown to reduce errors by a factor of two. However it is not strictly necessary and the current article focuses mainly on obtaining high-quality initial estimates.

This is important because it indicates that our careful low-level stereo image processing greatly reduces the computational burden (and to a certain extent the requirement) of full bundle adjustment. (This is of particular interest for platforms with limited computational resources such as phones.)

5 Relocalisation and loop closure

The method described above is generally successful in the normal course of operation. Nevertheless failures are almost inevitable, and there is a need for more resilient methods that enable the system to recover (i.e. relocalise) after such failures, as well to detect a return to previously mapped areas (i.e. loop closure). For both processes we make use of the SIFT descriptors computed on feature initialisation.

5.1 Relocalisation

The system uses a standard relocalisation mechanism when data association fails between consecutive frames. The "true scale" SIFT descriptors (Section 6) between the current and the previous frames are matched by direct comparison. 3-point-pose RANSAC (Fischler and

Bolles (1981)) is then applied to robustly find the pose of the platform. If this step fails, loop closure (Section 5.2) is attempted on subsequent frames. This approach takes advantage of the stereo setting and avoids the training and memory requirement of methods such as randomised trees (Lepetit and Fua (2006); Williams et al (2007)).

5.2 Loop closure

For loop closure we rely on fast appearance based mapping (Cummins and Newman (2008))[1]. This approach represents each place using the bag-of-words model developed for image retrieval systems in the computer vision community (Sivic and Zisserman (2003); Nistér and Stewenius (2006)). At time k the appearance map consists of a set of n_k discrete locations, each location being described by a distribution over which appearance words are likely to be observed there. Incoming sensory data is converted into a bag-of-words representation; for each location, a query is made that returns how likely it is that the observation came from that location's distribution or from a new place. This allows us to determine if we are revisiting previously visited locations.

FABMAP also returns possible feature matches that can be treated as normal matches in our visual processing pipeline. More specifically, we apply the robust localisation described in Section 4. E. and, if successful, we add a link in the graph containing this new estimate as in Fig. 2(b). The previous part of the map will then be automatically discovered by BFS and used for matching and localisation. This is how drift can be reduced through loop closure without requiring global estimation.

In a filtering framework, incorrect loop closures are often catastrophic as the statistical estimates are corrupted. Using the CRR representation, an incorrect loop closure would translate into attempting data association with landmarks from another part of the map. This could be detected as the robust estimator would reject most of the matches and a large proportion of tracked landmarks would be newly initialised landmarks. Once detected, the CRR enables recovery from erroneous loop closures as removing the incorrect graph link and bad measurements returns the system to its previous state.

[1] A version of FABMAP is available at `www.robots.ox.ac.uk/~mobile`

5.3 Key frames and localisation

When exploring environments over long periods of time, memory usage becomes an issue. The presented system uses a simple heuristic similar to that presented in (Mouragnon et al (2006)) to decide what frames to keep. Furthermore, when exploring a previously mapped area detected by loop closure, the system localises with respect to the active region thus reducing the amount of new features created and simultaneously reducing drift (Fig. 2(c) illustrates this mechanism). The metric for deciding when to connect poses is based on the distance (typically 1 m) and angle (10 deg) between frames and a minimum number of tracked landmarks (typically 50%).

6 True Scale

The well-known SIFT (Lowe (2004)) descriptor is built at a scale determined by finding an extremum in scale in a Difference of Gaussians (DoG) pyramid. The most expensive part of the algorithm is generally the computation of the image scale space. It has been shown to be feasible in real-time (Eade and Drummond (2008)) (without transferring the processing to a graphics card) using a highly optimised recursive Gaussian filter and a down-sampled image (320×240). In this work, we provide a different approach to scale invariance.

Previous work (Chekhlov et al (2007)) has also investigated solutions to avoid this cost in the case of monocular SLAM using the estimated camera pose. An alternative is proposed here for stereo pairs that avoids the knowledge of camera position. Landmark descriptors are built corresponding to regions in the world of same physical size - we call this the "true scale" of the feature. This provides the property of matching only regions of same 3-D size which is not necessarily the case with DoG features. It can be achieved at no extra computational cost as the left-right matching that provides the 3-D location is required in any case for the motion estimation. True scale requires choosing a set of 3-D sizes for different depth ranges to ensure the projection size of the 3-D template lies within a given pixel size range (Fig. 3).

We adopt a pinhole camera model with a focal length f. The size in the image of the projection of a 3-D region of space is inversely proportional to its distance to the centre of projection. Let s_{max} and s_{min} be the maximal and minimal size of square templates that could be matched reliably. s_{max} corresponds to a certain land-

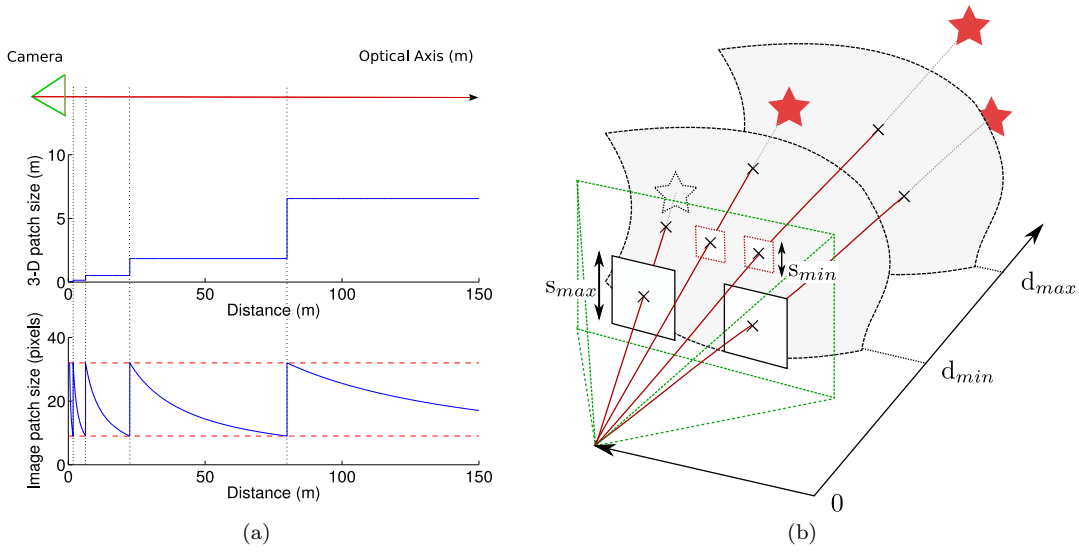

Fig. 3 True scale SIFT. (a) This figure shows the 3-D patch size in meters (middle graph) with respect to the distance from the camera centre (the camera is symbolised by a green triangle). The size of the patch projected in the image is shown in the bottom graph in pixels. The 3-D patch size has been computed using eq. (2). The reprojected size is within the chosen bounds s_{max} = and s_{min} = represented by the dashed red lines. The size of each band grows with the distance to the camera. (b) This figure illustrates a band with a fixed 3-D region size between distances d_{min} and d_{max}. Within this band, features represented by red stars project to template sizes ranging from s_{max} to s_{min} with size in $\frac{1}{d}$. For $d > d_{max}$, a bigger fixed 3-D size can be computed to provide image templates within the same pixel size range.

mark distance d_{min}. The maximal acceptable distance corresponding to s_{min} (Fig. 3(b)) is then:

$$\begin{cases} d_{max} = \frac{s_{max}}{f} \\ d_{min} = \frac{s_{min}}{f} \end{cases} \Rightarrow \quad d_{max} = \frac{s_{max}}{s_{min}} d_{min} \tag{1}$$

For typical values: d_{min} =0.5 m, s_{max} = 32 pixels and s_{min} = 9 pixels, d_{max} ≈1.8 m which is insufficient to cover the full depth range. A solution is to use different 3-D sizes in "bands" to cover the depth range. Figure 3(a) shows the different distance discontinuities in 2-D corresponding to s_{min} and s_{max} according to the distance to the camera. Figure 3(a) also illustrates the image template size according to depth. When relocalising or computing loop closures, only features belonging to the same band are matched as this ensures that only features corresponding to the same 3-D region are matched.

The different distances forming the bands can be computed from eq. 1 recursively. Let d_n be the smallest distance for band n, using geometric series:

$$\begin{cases} d_1 = d_{min} \\ d_{n+1} = \left(\frac{s_{max}}{s_{min}}\right) d_n \end{cases} \Leftrightarrow \begin{cases} d_{n+1} = \left(\frac{s_{max}}{s_{min}}\right)^n d_{min} \\ n \geq 0 \end{cases} \tag{2}$$

The template size as a function of the landmark distance, $s(d)$ can thus be computed from (taking the log of the left-hand side of 2):

$$\begin{cases} n = \lfloor \frac{\log(d/d_{min})}{\log(s_{max}/s_{min})} \rfloor + 1 \\ s(d) = s_{max} \left(\frac{d_n}{d}\right) \\ \quad\quad = s_{max} \left(\frac{s_{max}}{s_{min}}\right)^{n-1} \frac{d_{min}}{d} \end{cases} \tag{3}$$

Once the scale $s(d)$ has been estimated, a SIFT descriptor is built [2]. The image pyramid computed in Step A (Section 4) provides only a discrete set of scale values. To provide a close approximation of the appearance of the region at the scale $s(d)$, the descriptor is build on a patch computed by scaling and bilinear interpolation from the closest octave.

7 Experimental results

In this section we conduct quantitative and qualitative evaluations of our system on both synthetic and real sequences. We assess the accuracy of our method, and consider the impact of the various front-end image processing operations with regard to accuracy and robustness. In particular we make comparisons with a current state-of-the-art monocular system in various environments.

[2] The SIFT implementation is based on the code provided by A. Vedaldi and B. Fulkerson (Vedaldi and Fulkerson (2008)).

(a) Begbroke aerial view (b) New College aerial view

Fig. 4 Outdoor sequences.

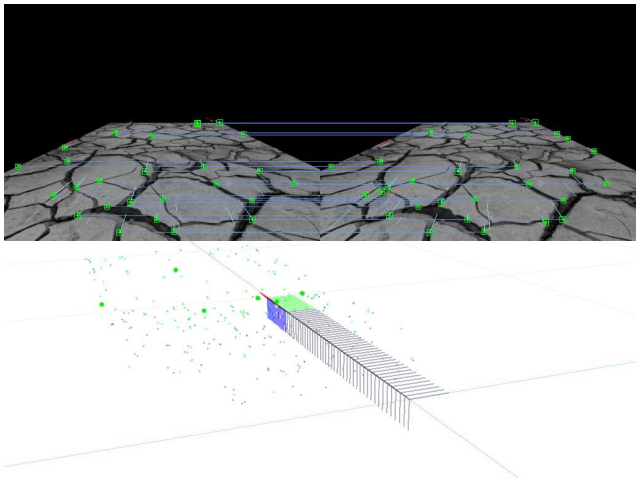

Fig. 5 Image of the simulation setup

Video of our system running on both indoor and outdoor sequences is available on the authors' website. It exhibits the system's behaviour in presence of motion blur, fog, lighting changes, lens flare and dynamic objects.

7.1 Simulation

The simulation setup consists of 50 stereo frames generated in a straight line and spaced every 20cm with a 10cm baseline. Changes in illumination or automatic camera intensity settings were simulated by adding a global intensity offset to all image values drawn from a Gaussian distribution with a standard deviation of 15. Sensor noise was simulated by adding random intensity values drawn independently from a Gaussian distribution with a standard deviation of 2.

In order to assess the accuracy of the system we compare the pose estimate with ground truth and integrate the (absolute) difference along the entire path length. Note that this is different from simply comparing the estimated end location against the ground truth end location, since the latter may incorporate errors which cancel, and also has the drawback that if the system operates in a finite environment, the error is bounded by the size of the environment (consider a system that simply travels in a small circle; its end-point error will be bounded by the diameter of the circle). Figure 5 shows the final images of the sequence and the estimated path.

Figures 6(a)-6(e) show the precision obtained for different numbers of landmarks and the effect of two different aspects of the system: (a) data association using subpixel minimisation and (b) motion estimation using the map and not only frame-to-frame tracking (as in visual odometry). The results show that tracking 100-150 landmarks with subpixel minimisation leads to a precision of about 9cm per 100m or about one metre per kilometre. This precision was also observed on real data in good conditions (small amounts of blur and a good feature distribution). Without subpixel minimisation, the error increased by a factor of three. This simulation combined with experiments on real data confirm the importance of subpixel data association to obtain precise estimates.

Visual odometry (VO) consists in removing step D in Section 4 from the visual processing steps. We found that the precision was not reduced (and even appears as slightly better towards the end because of the accumulation of error in the 3-D landmark estimates with respect to the latest pose). The good quality of VO can be explained by the precise estimates from subpixel minimisation but also the strong constraints provided by the stereo pair (in contrast to a monocular system). One noticeable effect of not using the map was in the robustness of the tracking. Tracking failure occurred when fewer than 40 landmarks were used.

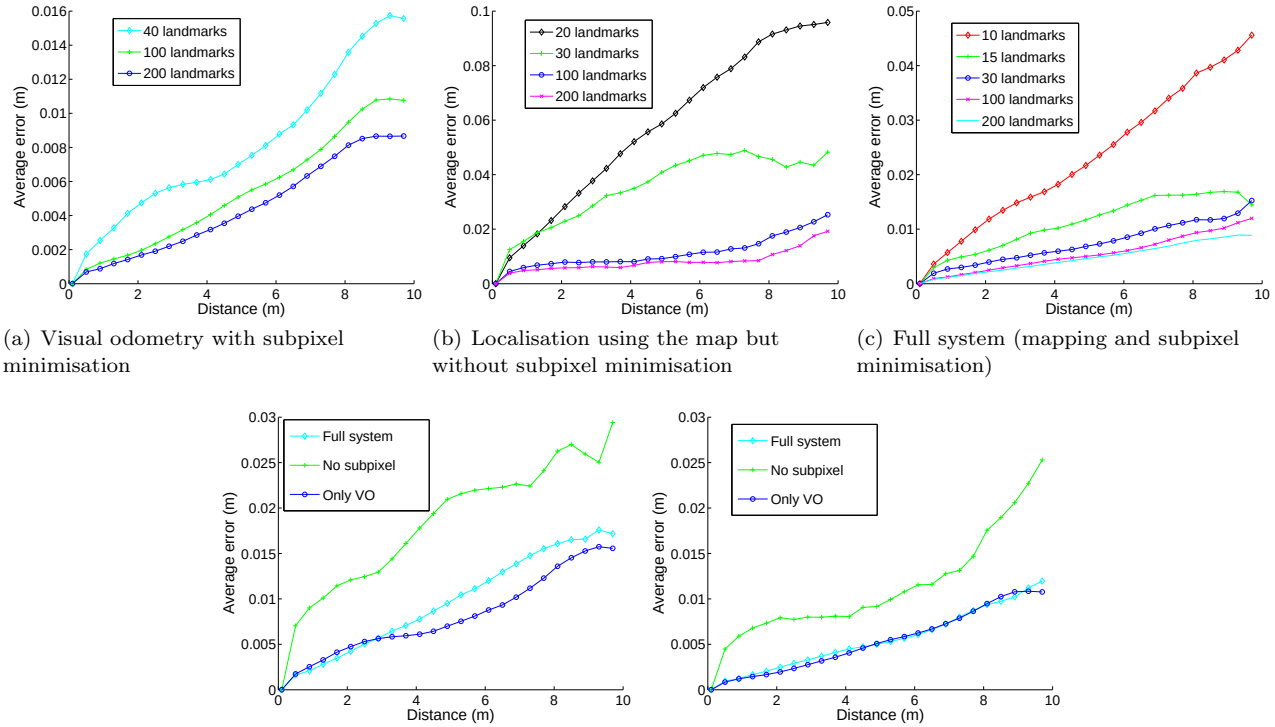

(a) Visual odometry with subpixel minimisation

(b) Localisation using the map but without subpixel minimisation

(c) Full system (mapping and subpixel minimisation)

(d) Effect on system performance of the different components for 40 landmarks

(e) Effect on system performance of the different components for 100 landmarks

Fig. 6 Simulation of the effect of the different system components and the number of landmarks on the translation error. Three cases are analysed: (i) *visual odometry (VO)*, where the map is not used for localisation and only frame-to-frame estimation is done (but with subpixel minimisation for data association) (ii) *no subpixel*, where the map is used for localisation but we do not use SSD gradient descent to provide subpixel data association and (iii) *full system*, where all the components of the system are used in particular the map and subpixel minimisation. Figure (a) shows the system when localisation with respect to the map is not performed. The precision is similar to when using the map but tracking failure is more likely to occur. Figure (b) shows the system without subpixel minimisation. The final error increases by a factor of three. Figure (c) shows the results using the full system. The precision for 100-150 features is about 1m for 1km. Figures 6(d) and 6(e) show the translation error for 40 and 100 landmarks with and without subpixel minimisation and mapping. Subpixel minimisation greatly improves precision. The precision obtained when using the map or only using visual odometry is similar but the tracking failed when fewer than 40 landmarks were tracked with only visual odometry.

	Begbroke	New College
Distance Travelled	1.08 km	2.26 km
Frames Processed	23K	51K
Reprojection Error Min/Avg/Max	0.003 / 0.17 / 0.55 pixels	0.03 / 0.13 / 1.01 pixels
Accuracy without loop closure	∼1m in (x-y) plane, ∼1m in z	∼15-25m in (x-y) plane, ∼15m in z
Accuracy with loop closure	∼1cm in (x-y) plane, ∼1cm in z	∼10cm in (x-y) plane, ∼10cm in z

Table 1 Results for the Begbroke and New College data sets.

7.2 Outdoor sequences

The full system was tested on numerous real sequences of up to 2km. A total of 5km was traversed and over 300K images processed. In this work, the vocabulary used for FABMAP contained 10000 words generated from a separate sequence of 11200 frames.

The performance on two specific sequences acquired at 20Hz and shown in Fig. 4(a) and 4(b) are detailed in Tab. 1. The estimated trajectories can be found in Fig. 7[3]. No ground truth is available for these two sequences but the robot was driven so that its trajectory would overlap. The accuracy reported in the table was measured in the x-y plane and along the z-axis with and without loop closure. Even without a global relaxation, loop closure greatly improves the accuracy.

[3] The New College dataset set is available online at `www.robots.ox.ac.uk/NewCollegeData/` (Smith et al (2009)).

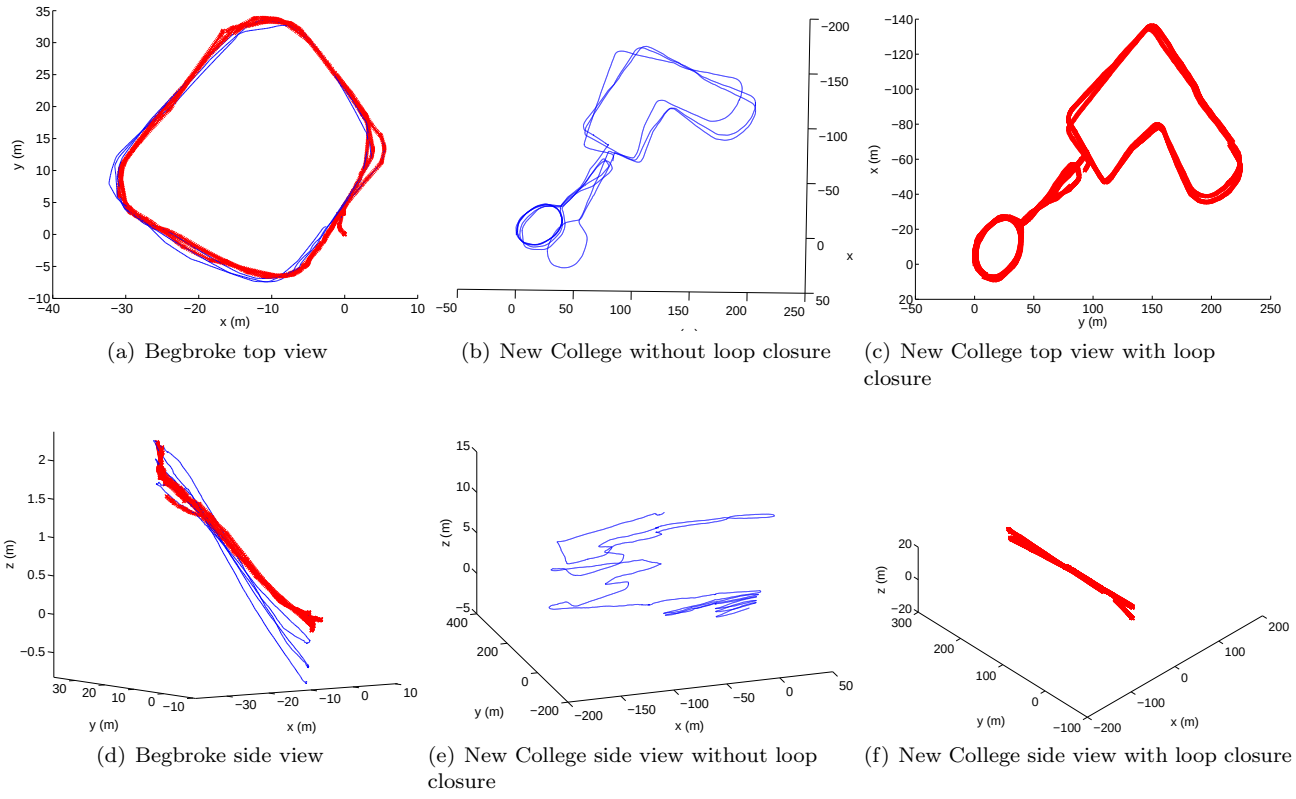

(a) Begbroke top view (b) New College without loop closure (c) New College top view with loop closure

(d) Begbroke side view (e) New College side view without loop closure (f) New College side view with loop closure

Fig. 7 Estimated trajectories for the data sets detailed in Tab. 1 containing three loops. The trajectories are shown processed with loop closure (red trajectory with crosses) and without (blue continuous line).

7.3 Indoor sequence

The system was tested on the "Atrium" indoor sequence shown in Fig. 8(a). This short sequence acquired at walking pace contains around 2K frames and was chosen as: (a) it exhibits clear structure that provides a visual indication of the quality of the estimates and (b) it is a challenging environment exhibiting regions with little texture but also regions with repeated patterns. Figure 8 shows two views of the estimated map and trajectory. The alignment of the two staircases and the structure of the floor is an indication of a good quality estimate.

In this difficult setup, the stereo pair proved particularly useful as the data association provided by the scanline search simplified the data association.

7.4 Robustness assessment and comparison to PTAM

In order to provide a qualitative assessment of the benefits of our system, particularly the carefully engineered vision front-end, we have compared it to a current state-of-the-art monocular system, Parallel Tracking And Mapping (PTAM) (Klein and Murray (2007)) using the source code available online[4]. This comparison highlights the importance of the different processing steps proposed in this article to provide robustness to varying conditions in indoor and outdoor environments.

PTAM and the proposed system have different objectives that have influenced the choice of the underlying algorithms. PTAM aims to provide a 3-D representation of the world for augmented reality (AR) for a small indoor workspace. RSLAM is aimed at both indoor and outdoor applications that have lead us to include mechanisms to deal with strong changes in illumination and low contrast (Section 4.B) and provide a good distribution of features in the image (Section 4.F). The choice of a stereo pair was also motivated by the ease of map initialisation and in particular to avoid the problem of unobservability common to all monocular systems; a pure rotation is a typical failure mode of a monocular system since it provides no triangulation baseline.

The PTAM system has a similar image processing pipeline but requires a "bootstrapping" designed to build an initial map that can be tracked and also optimised using bundle adjustment in a background

[4] PTAM can be downloaded at `http://www.robots.ox.ac.uk/~gk/PTAM/`

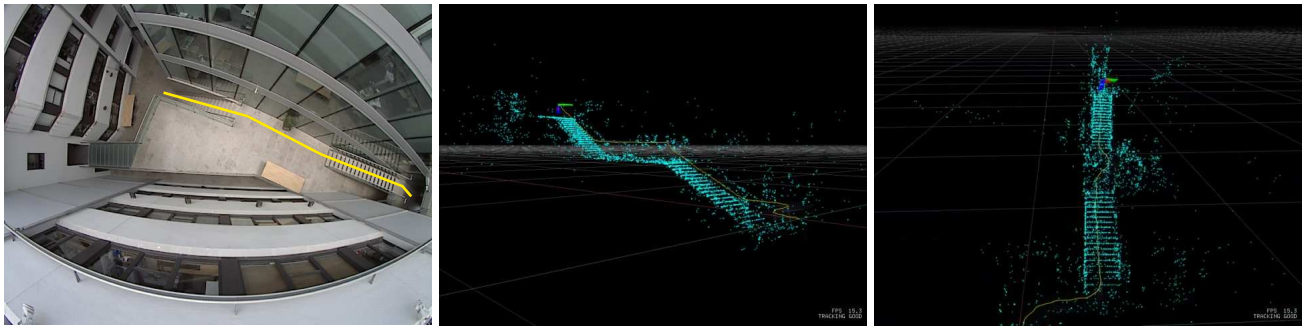

(a) Atrium aerial view (b) Atrium side view (c) Atrium top view

Fig. 8 Atrium sequence. (a) shows a top view of the atrium and the trajectory taken (b) and (c) show the estimated trajectory and map for the atrium indoor sequence. The structure of the steps are apparent. The first floor appears parallel to the ground and the staircase are aligned indicating that the pose and map are correctly estimated.

thread. The initialisation phase requires a user to move the camera to create a baseline. This phase is acceptable for an AR application but is obviously a drawback for applications such as robotics. A stereo system does not require this step as the baseline is known at the start which greatly simplifies the initialisation of features (Section 4.F).

PTAM was tested on the outdoor Begbroke sequence, the indoor Atrium sequence and in an office-like environment. Different parameters of the PTAM software were tested: distance between keyframes, coarse and fine search regions for data association during tracking, rotation initialisation for coarse search and increasing the computational time to allow better precision from the bundle adjuster. The only parameter that improved significantly the performance from the default values was the distance between keyframes. This parameter depends on the initial map scale generated from the baseline during initialisation. This value is set to a sensible value (10cm in the program) for AR but is not adequate for outdoor sequences where the scales are different.

We will start by describing the main difficulties encountered and will then describe which sequences in particular were affected. The following three main difficulties rendered the mapping particularly challenging for the monocular system:

1. **initialisation**. It was difficult to find a sequence of images that provided a good initialisation for the system in the Begbroke and Atrium sequences. For example the motion at the start of the Begbroke sequence is close to a pure rotation and few features could be extracted on the ground.
2. **poor feature distribution**. As shown in Figure 9, imposing a good distribution of features is particularly important with images containing high frequency produced for example from vegetation to avoid poor trajectory estimates. PTAM does not have such a mechanism which had a strong impact not only at initialisation but also for subsequent tracking. Figure 10(a) illustrates the features extracted with a fixed threshold as in PTAM. Figure 10(e) shows the result obtained by RSLAM.
3. **changes in illumination**. In Section 4.B, a simple mechanism was proposed to adapt the feature extraction threshold to changes in illumination and low contrast. PTAM does not provide such a method and the tracking failed on sequences with low contrast as in Fig. 10.

We did not test PTAM with loop closure. PTAM requires precise global 3-D estimates to provide accurate image reprojections for the tracking. At loop closure, this would be problematic as projecting previous parts of the map requires a costly bundle adjustment that is not real-time and grows cubicly with the number of frames in the map. This is where a relative representation would be beneficial.

The tests on the three sequences provided the following outcome:

1. **Begbroke sequence.** The Begbroke sequence proved particularly challenging for the PTAM system. On about 80% of this sequence, the system failed due a mixture between initialisation issues, poor feature distributions or lack of features due to low contrast. The longest continuous set of frames tracked by PTAM is comprised of around 800 frames over a distance of about 40m. On this part of the sequence, both systems provided a similar precision as shown in Fig. 11(a) (the relative scale was estimated by minimising the trajectory difference).
2. **Indoor environment.** In this experiment the camera used has a larger field of view (100 deg instead of 65 deg), the ambient illumination did not change greatly, and the distribution of features did not prove

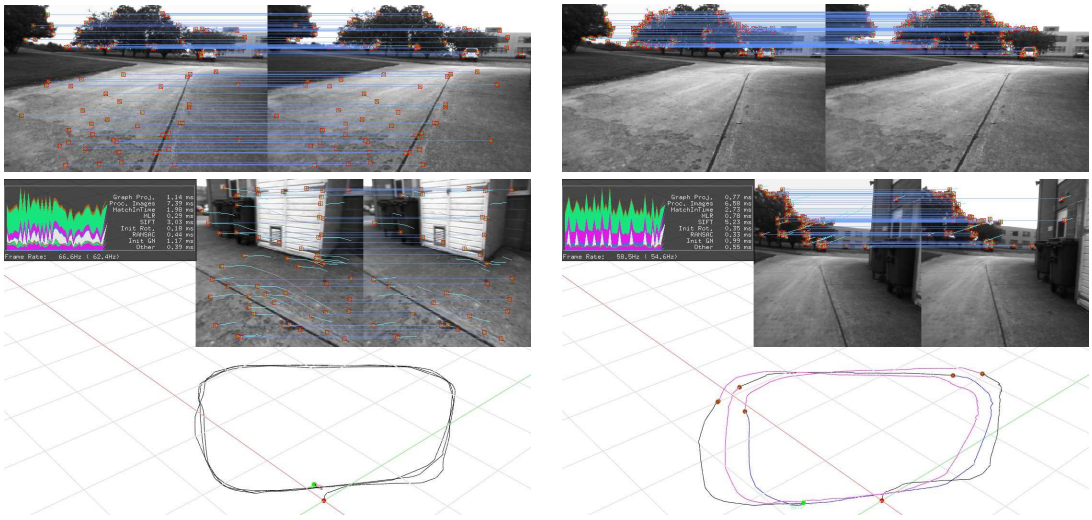

(a) (b)

Fig. 9 Importance of quadtrees to provide a good feature distribution. These figures show the estimated trajectory for the Begbroke sequence using (a) the full system and (b) the system without quadtree feature selection. Taking the strongest Harris scores as in Fig. (b) can lead to poorly constrained motion estimates. In the present case, the vegetation provides many strong Harris corners but leads to a poor feature distribution. Figure (a) illustrates that using a quadtree can provide a distribution of features that does not necessary have the best Harris scores but provides strong constraints for motion estimation.

(a) Features extracted with a standard threshold on a low contrast image.

(b) Features extracted with an automatically adapted threshold on a low contrast image.

(c) Best 100 features. These features are similar irrespective of the extraction threshold.

(d) Extracted features with constrained distribution and a standard threshold.

(e) Extracted features with constrained distribution and an adapted threshold.

Fig. 10 Example of an image with low contrast in the Begbroke sequence (Fig. 4(a)). The tracking in PTAM failed as the feature extraction threshold is fixed and too high for this image as shown in Fig. 10(a). However simply reducing the threshold is not sufficient as the features will suffer from a poor distribution as illustrated in Figures 10(b),10(c). It is by combining a mechanism to ensure a good distribution of features and a mechanism to adapt the threshold that it is possible to track in this situation Fig. 10(e).

critical. For these reasons PTAM is better suited to this environment and consequently the results were better than for the outdoor sequence. Nevertheless PTAM still exhibited a number of failures where our system successfully tracked the entire sequence. PTAM was able to track two separate sections (Fig. 8): from the bottom of the atrium to the middle of the first flight of stairs and from first floor to the middle of the second staircase. The spatial aliasing combined with low precision lead to incorrect data association and tracking failure on the stairs (Fig. 11(b)). The estimated precision of the landmarks on the staircase was poor because of the small number of measurements and the small baseline.

3. **Desktop environments.** We also compared the systems in a smallish desk and office space. Since this is the environment for which PTAM was designed, unsurprisingly it produced an accurate map with stable tracking. As reported in (Klein and Murray (2007)), the quality was improved when using the larger field of view camera (100 deg instead of 65 deg). Our system was also able to build a good quality map but close zoom-ins were not possible as the system only initialises features that have left-right correspondences (Section 4.F).

In conclusion, the empirical evidence of these experiments points to the importance for robust camera tracking of careful engineering to compensate for changes in lighting and of ensuring a good distribution of features. Our solution based on quadtrees is heuristic but effective. While these aspects could readily be incorporated in a monocular system as well, we have also shown the

(a) Comparison of the trajectories produces by PTAM and RSLAM on the longest continuous set of frames tracked by PTAM on the Begbroke sequence. It is comprised of around 800 frames or about 40m. The trajectory estimated by PTAM is in blue with circles and the one estimated by RSLAM is in red with crosses. The accuracy was similar for both systems.

(b) Stairs generated spatial aliasing in the Atrium sequence. This lead to failures in tracking for the PTAM system. Using a stereo pair increases the precision of the map, rendering the RSLAM system overall more robust (although not immune) to spatial aliasing.

Fig. 11 Elements of comparison of PTAM and RSLAM on the Begbroke sequence (Fig. 8) and the Atrium sequence (Fig. 8(a)).

Times (ms)	Min	Avg	Max
Pre-processing	7.6	11.9	29.8
Tracking	1.4	3.8	10.0
RANSAC	0.1	0.3	3.4
Localisation	0.9	3.2	14.8
Left-right matching	0.0	1.5	5.4
SIFT descriptors	1.0	6.1	12.6
Total	15.3	26.8	49.7

Table 2 Breakdown of the processing time without loop closure. The system runs on average at 37Hz. The variability is due to the number of features tracked at a given time and the number of landmarks projected through the graph.

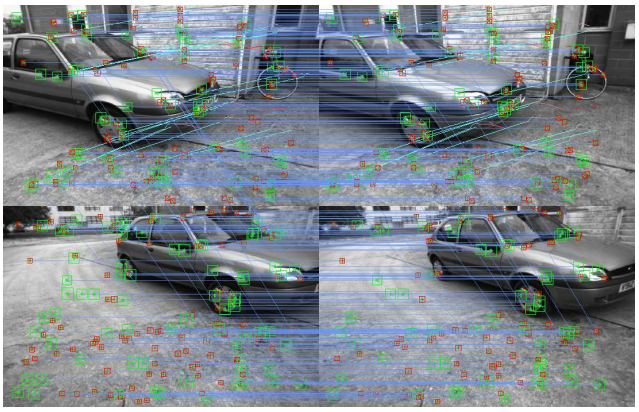

Fig. 14 The inter-frame motion between these stereo images lead to tracking failure when using FAST and SAD matching. However using true-scale SIFT, we obtain the depicted matches that provide an accurate position estimate.

value inherent in a binocular view, which automatically overcomes one of the main failure modes of monocular methods.

7.5 Overall performance

The average computation time without loop closure on an Intel 2.40GHz Quad CPU with only one core running totals 27ms (∼37Hz). When only computing SIFT features on key frames (Section 5.3), the average frame-rate increases to 44Hz. A breakdown can be found in Tab. 2. Only a single frame from the entire 23000 frames (20 min.) used more than the maximum available frame-rate budget of 50ms.

To summarise, the following components contributed to the overall performance:

1. **Quadtrees** Figure 9 shows how quadtrees affect the spreading of features for outdoor sequences. Vegetation typically gives strong Harris corner responses but often poorly constrains the estimates.
2. **Sub-pixel refinement** Sub-pixel refinement was found to be essential to obtain precise trajectory estimates as shown in Fig. 12.
3. **Multi-level quadtrees** Robustness to motion blur can be improved by using quadtrees over 2-4 image pyramid levels. Figure 13 illustrates the effect of pyramid levels on feature extraction.
4. **Changes in illumination** A simple mechanism to compensate for changes in illumination and low contrast proved important in outdoor sequences (Fig. 10).
5. **Loop closures** Figures 7(a)-7(f) show the results with and without loop closure. Loop closure substantially reduces drift without requiring a global minimisation. While the loop closure mechanism is not strictly constant time, 103K keyframes were pro-

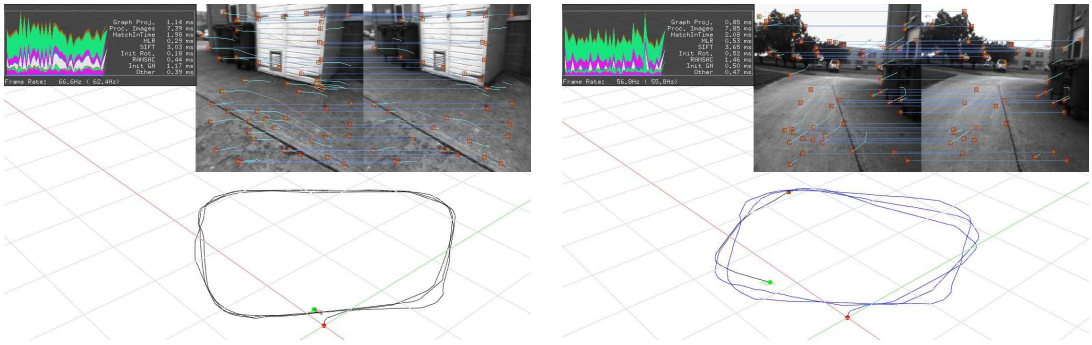

(a) (b)

Fig. 12 Importance of subpixel data association. These two figures show the estimated trajectory for the Begbroke sequence using (a) the full system and (b) the system without subpixel minimisation. Without subpixel minimisation, the precision is greatly reduced.

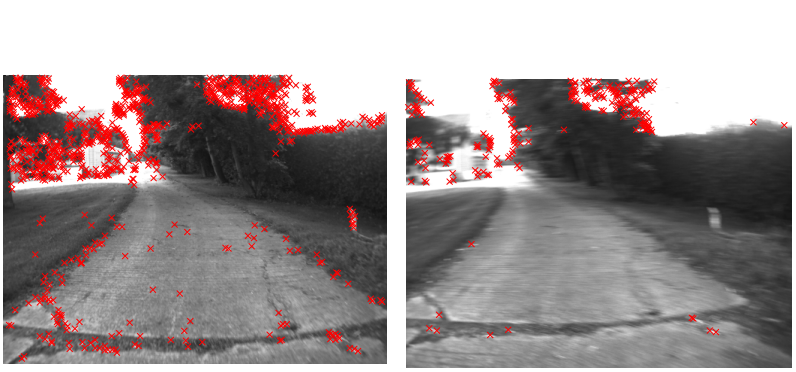

(a) FAST corners extracted in an image without blur.

(b) FAST corners extracted in an image with blur.

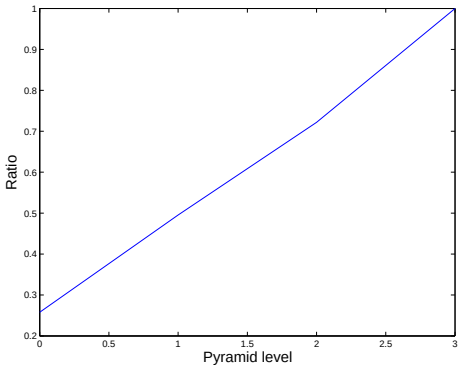

(c) Ratio between the number of features extracted in the blurred and non-blurred images versus pyramid level.

Fig. 13 The number of FAST corners extracted for a given threshold diminishes in presence of blur as illustrated by the non-blurred and blurred images of the same scene in Fig. 13(a) and Fig. 13(b). This can be explained by the low-pass filter effect of motion blur that reduces the high frequency information on which FAST corners rely. Figure 13(c) shows the benefit of combining pyramid levels with feature extraction. As the pyramid level increases, the number of extracted features becomes similar and the ratio tends to 1.

cessed with a maximum processing time for any observation of 44.1 ms.

6. **True scale descriptors** The use of rich (SIFT) descriptors greatly improves the robustness. Since their use incurs additional computational cost, they are only used as fallback in difficult conditions when FAST corners combined with SAD do not provide enough correct matches for localisation. Much of this cost is mitigated through use of our proposed true scale obtained from the true feature depth, rather than the image-based scale more usually used. Figure 14 shows an example where true scale SIFT was required for successful matching after failure of the simpler but faster FAST plus SAD approach.

8 Conclusion

This paper described a relative stereo SLAM system that demonstrated how a continuous relative representation combined with careful engineering (true scale, subpixel minimisation and quadtrees) can provide constant-time precise estimates, efficiency and good robustness. This framework is more than a simple re-parametrisation of the map and trajectory as it leads to a different cost function. It is possible to represent trajectories that cannot be embedded in a Euclidean space - an assumption common to most previous work.

Acknowledgements The work reported in this paper undertaken by the Mobile Robotics Group was funded by the Systems Engineering for Autonomous Systems (SEAS) Defence Technology Centre established by the UK Ministry of Defence, Guidance Ltd, and by the UK EPSRC (CNA and Platform Grant EP/D037077/1). Christopher Mei and Ian Reid of the Active Vision Lab acknowledge the support of EPSRC grant GR/T24685/01. This work has partly been supported by the European Commission under grant agreement number FP7-231888-EUROPA.

References

Bailey T, Durrant-Whyte H (2006) Simultaneous Localisation and Mapping (SLAM): Part II - State of the Art. Robotics and Automation Magazine

Benhimane S, Malis E (2004) Real-time image-based tracking of planes using efficient second-order minimization. In: IEEE International Conference on Intelligent Robots and Systems, Sendai, Japan, vol 1, pp 943–948

Bosse M, Newman P, Leonard J, Teller S (2004) Simultaneous Localization and Map Building in Large-Scale Cyclic Environments Using the Atlas Framework. The International Journal for Robotics Research 23(12):1113–1139

Castellanos J, Neira J, Tardós J (2004) Limits to the consistency of EKF-based SLAM. In: Proceedings of the Fifth IFAC Symposium on Intelligent Autonomous Vehicles, Lisbon, Portugal

Chekhlov D, Pupilli M, Mayol W, Calway A (2007) Robust Real-Time Visual SLAM Using Scale Prediction and Exemplar Based Feature Description. In: IEEE Conference of Vision and Pattern Recognition, Minneapolis, USA, pp 1–7

Chli M, Davison AJ (2008) Active Matching. In: European Conference on Computer Vision, Marseille, France, vol 5302/2008, pp 72–85

Cummins M, Newman P (2008) FAB-MAP: Probabilistic Localization and Mapping in the Space of Appearance. The International Journal for Robotics Research 27(6):647–665

Davison AJ (2003) Real-Time Simultaneous Localisation and Mapping with a Single Camera. In: IEEE International Conference on Computer Vision

Davison AJ, Reid I, Molton N, Stasse O (2007) Monoslam: Real-time single camera slam. IEEE Transactions on Pattern Analysis and Machine Intelligence 29(6):1052–1067

Durrant-Whyte H, Bailey T (2006) Simultaneous Localisation and Mapping (SLAM): Part I The Essential Algorithms. Robotics and Automation Magazine

Eade E, Drummond T (2007) Monocular SLAM as a Graph of Coalesced Observations. In: IEEE International Conference on Computer Vision, Rio de Janeiro, Brazil, pp 1–8

Eade E, Drummond T (2008) Unified Loop Closing and Recovery for Real Time Monocular SLAM. In: British Machine Vision Conference, Leeds, UK

Fischler MA, Bolles RC (1981) Random sample consensus: a paradigm for model fitting with applications to image analysis and automated cartography. Commun ACM 24(6):381–395

Hartley R, Zisserman A (2000) Multiple View geometry in Computer vision. Cambridge university press

Julier S, Uhlmann J (2001) A counter example to the theory of simultaneous localization and map building. Robotics and Automation 4:4239–4243

Klein G, Murray D (2007) Parallel Tracking and Mapping for Small AR Workspaces. In: IEEE and ACM International Symposium on Mixed and Augmented Reality, Nara, Japan

Konolige K, Agrawal M (2008) Frameslam: From bundle adjustment to real-time visual mapping. IEEE Transactions on Robotics 24(5):1066–1077

Lepetit V, Fua P (2006) Keypoint recognition using randomized trees. IEEE Transactions on Pattern Analysis and Machine Intelligence 28(9):1465–1479

Lowe DG (2004) Distinctive image features from scale-invariant keypoints. International Journal of Computer Vision 2(60):91–110

Mei C, Benhimane S, Malis E, Rives P (2008) Efficient Homography-Based Tracking and 3-D Reconstruction for Single-Viewpoint Sensors. IEEE Transactions on Robotics 24(6):1352–1364

Moore DC, Huang AS, Walter M, Olson E, Fletcher L, Leonard J, Teller S (2009) Simultaneous Local and Global State Estimation for Robotic Navigation. In: IEEE International Conference on Robotics and Automation, Kobe, Japan, pp 3794–3799

Mouragnon E, Lhuillier M, Dhome M, Dekeyser F, Sayd P (2006) Real-Time Localization and 3D Reconstruction. In: IEEE Conference of Vision and Pattern Recognition, New York, USA, vol 1, pp 363–370

Nistér D, Stewenius H (2006) Scalable recognition with a vocabulary tree. In: IEEE Conference of Vision and Pattern Recognition, New York, USA, vol 2, pp 2161–2168

Nistér D, Naroditsky O, Bergen J (2006) Visual Odometry for Ground Vehicle Applications. Journal of Field Robotics 23(1)

Rosten E, Drummond T (2005) Fusing points and lines for high performance tracking. In: IEEE International Conference on Computer Vision, Beijing, China, vol 2, pp 1508–1515

Sibley G, Mei C, Reid I, Newman P (2009) Adaptive Relative Bundle Adjustment. In: Robotics: Science and Systems, Seattle, USA

Sivic J, Zisserman A (2003) Video Google: A Text Retrieval Approach to Object Matching in Videos. In: IEEE International Conference on Computer Vision, Nice, France, vol 2, pp 1470–1477

Smith M, Baldwin I, Churchill W, Paul R, Newman P (2009) The new college vision and laser data set. The International Journal for Robotics Research 28(5):595–599

Thrun S, Burgard W, Fox D (2005) Probabilistic Robotics. MIT Press

Triggs B, McLauchlan PF, Hartley RI, Fitzgibbon AW (1999) Bundle adjustment – a modern synthesis. In: Vision Algorithms: Theory and Practice: International Workshop on Vision Algorithms, Computer Science, Springer Berlin / Heidelberg

Vedaldi A, Fulkerson B (2008) VLFeat: An open and portable library of computer vision algorithms. `http://www.vlfeat.org`

Williams B, Klein G, Reid DI (2007) Real-time slam relocalisation. In: IEEE International Conference on Computer Vision, Rio de Janeiro, Brazil, pp 1–8